IOP Publishing and International Atomic Energy Agency Nuclear Fusion
Nucl. Fusion **52** (2012) 074013 (9pp) doi:10.1088/0029-5515/52/7/074013

Influence of rotating resonant magnetic perturbation on the plasma radial electric field on TEXTOR

T. Zhang[1,5], Y. Liang[1], Y. Sun[1], A. Krämer-Flecken[1], S. Soldatov[1,2], E. Nardon[3], P. Tamain[3], F.L. Waelbroeck[4], Y. Yang[1,5], J. Pearson[1], H.R. Koslowski[1] and the TEXTOR team

[1] Institute of Energy and Climate Research-Plasma Physics, Forchungszentrum Jülich GmbH, Association EURATOM-FZJ, Jülich, Germany[a]
[2] Department of Applied Physics, Ghent University, 9000 Ghent, Belgium
[3] Association EURATOM/CEA, CEA Cadarache, F-13108, St Paul-lez-Durance, France
[4] Institute for Fusion Studies, The University of Texas, Austin, TX 78712, USA
[5] Institute of Plasma Physics, Chinese Academy of Sciences, PO Box 1126, Hefei, Anhui 230031, People's Republic of China

E-mail: zhangt@ipp.ac.cn

Received 17 October 2011, accepted for publication 23 March 2012
Published 5 July 2012
Online at stacks.iop.org/NF/52/074013

Abstract
The plasma radial electric field (E_r) has been changed by applying an $n = 1$ counter-rotating resonant magnetic perturbation (RMP) field with a frequency of 5 kHz in ohmic plasmas on TEXTOR. The change in the E_r (ΔE_r) is negative, different from the observations in previous experiments where ΔE_r was always positive when a static or low frequency (~1 kHz) rotating RMP field was applied in the plasma on TEXTOR. The E_r profile in the present experiment shows two distinct evolution stages. In the first stage, ΔE_r from the $q = 2$ to $q = 3$ surfaces have a similar decrease as the amplitude of the 5 kHz counter-rotating field increases. In the second stage, the decrease rate of ΔE_r is faster for the positions closer to the $q = 2$ surface. As a result, the E_r around the $q = 2$ surface has a significant change in this second stage while no change of E_r is observed near the $q = 3$ surface even after the excitation of an $m/n = 2/1$ tearing mode. A reduced MHD code, 4FC, has been used to model the experiment. Two simulations have been performed. The first one is by applying a single 2/1 perturbation while both, 2/1 and 3/1 perturbations, have been applied in the second simulation. The result from the second simulation is qualitatively consistent with the experimental observations while the first simulation including only a single 2/1 perturbation cannot explain the evolution of the E_r profile in the second stage as observed in the experiment.

(Some figures may appear in colour only in the online journal)

1. Introduction

In recent years, the resonant magnetic perturbation (RMP) field has been used for an active control of the edge-localized mode [1–3] or for the study of the field penetration [4, 5]. It has been observed in these experiments that the plasma rotation or radial electric field (E_r) can be changed with the application of the RMP field. The radial electric field plays an important role in magnetically confined plasma. Firstly, the E_r (or rotation) itself can stabilize the MHD instabilities. Secondly, the E_r shear can suppress the small scale plasma turbulence and thus improve the plasma confinement [6]. It is important to study how the RMP field changes the radial electric field and to investigate the mechanism responsible for this E_r change.

The TEXTOR tokamak has been equipped with the dynamic ergodic divertor (DED) [7] in order to study the interaction between the RMP field and plasma transport and stability. The DED consists of 16 in-vessel coils, which wind helically around the inner side of the torus with a pitch corresponding to the magnetic field lines on the magnetic flux surface with a safety factor (q) of 3. A static, co-rotating or counter-rotating RMP field with a frequency up to 10 kHz can be induced by the DED. Here, the co-rotating field means that the DED-field rotates in the ion diamagnetic drift (IDD) direction, i.e. in the co-current direction toroidally while the counter-rotating field indicates a perturbation rotating in the electron diamagnetic drift (EDD) direction, i.e. in the counter-current direction toroidally. The base mode numbers of the DED-field can be selected as $m/n = 12/4$, 6/2 and 3/1 by

[a] Partner in the Trilateral Euregio Cluster.

changing the coil connections to the power supply. In the $m/n = 3/1$ configuration, where the present experiment is conducted, the DED produces a perturbation with a toroidal mode number (n) of 1 and poloidal mode numbers (m) in the range 1–6 [8].

The previous experiments on TEXTOR have shown that when a static, co-rotating or counter-rotating RMP field with a frequency of about 1 kHz was applied in plasma, the change in the toroidal rotation was always in the co-current direction, as long as the tearing mode was not excited [5, 9]. This rotation change has been attributed to the stochastization of the magnetic fields in the plasma edge after the application of the RMP field. The enhanced radial transport of the electrons in the stochastic region leads to a charge separation which is counteracted by the buildup of a positive radial electric field. The measurements of the radial electric field by Langmuir probes [10] and a poloidal correlation reflectometry (PCR) [11] showed that the change in the E_r was actually positive after applying the RMP field in these experiments.

In this work, a counter-rotating RMP field with a frequency of 5 kHz, induced by the DED in the $m/n = 3/1$ configuration, has been applied in ohmic plasmas. It was found that the change in E_r, measured by the PCR [12–14], is negative with the application of the 5 kHz counter-rotating field. This E_r change is different from those observed in previous experiments on TEXTOR as discussed in the last paragraph. To further understand the mechanism responsible for this E_r change, the experimental results have been compared with the simulation performed by a reduced cylindrical MHD code, 4FC [15].

This paper is organized as follows: in section 2, we briefly describe the experimental setup and present the experimental results. The comparisons between experiment and simulation are given in section 3 followed by a discussion in section 4. We conclude in section 5.

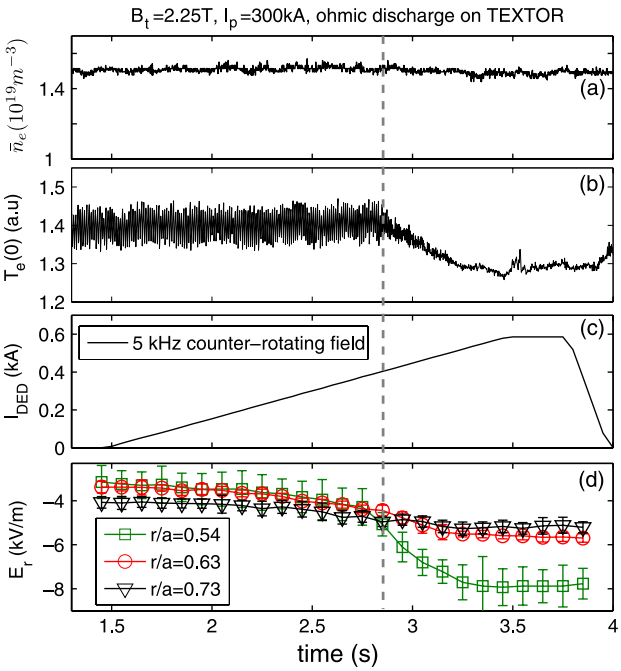

Figure 1. Overview of the experiment: (a) core line-averaged density $\bar{n}_e$, (b) the ECE signal measured in the plasma core $T_e(0)$, (c) the amplitude of the 5 kHz counter-rotating field induced by the DED in the $m/n = 3/1$ configuration, (d) the evolutions of the radial electric field (E_r), measured by the PCR, at three different radial positions. The vertical dashed line indicates the time of an $m/n = 2/1$ mode excitation.

2. Experimental setup and results

2.1. Experimental setup

The experiment presented here was performed on the TEXTOR tokamak. TEXTOR is a circular, medium sized, limiter tokamak with a major radius (R_0) of 1.75 m and a minor radius (a) of 0.47 m. A counter-rotating RMP field with a frequency of 5 kHz, produced by supplying ac currents to the DED coils in the $m/n = 3/1$ configuration, has been applied in ohmic plasmas (figure 1) with a toroidal magnetic field (B_t) of 2.25 T, a plasma current (I_p) of 300 kA and a core line-averaged electron density ($\bar{n}_e$) of 1.5×10^{19} m^{-3}. In these plasmas, the $q = 2$ surface is at about $r/a = 0.59$ while the $q = 3$ surface is at about $r/a = 0.78$ (figure 3(b)).

An O-mode PCR for the measurement of plasma density fluctuation is available on TEXTOR [11–14]. Reflectometry is based on a radar technique in which a microwave beam is directed into the plasma with the wave reflected from the cutoff layer. For O-mode reflectometry, the cutoff position is determined by the electron density (n_e). The PCR on TEXTOR operates in a frequency band of 26 GHz $\leqslant f \leqslant$ 40 GHz, corresponding to an electron density range 0.8×10^{19} m$^{-3} \leqslant n_e \leqslant 2.0 \times 10^{19}$ m^{-3}, and it is composed of three antenna arrays. Two of these arrays are at the equatorial plane in the low-field side and the third one is on top of the toroidal vessel. This top array, used in this experiment, is composed of one launcher and four poloidally and toroidally separated receivers, from which the density fluctuations have been measured at four adjacent points on the same magnetic flux surface. Here, we have assumed that the electron density on the same magnetic flux surface is homogeneous. The turbulence propagation time from one point to another one can be derived from the shift of the maximum of the cross-correlation function of the fluctuation signals measured by PCR. It is generally accepted that the drift wave turbulence in tokamak plasma has a much longer parallel correlation length compared with the perpendicular correlation length [16]. Therefore, the propagation time calculated using the cross-correlation technique is mainly due to the turbulence rotation perpendicular to the magnetic field. The perpendicular rotation ($v_\perp^{\rm turb}$) of the turbulence has been calculated from the propagation time [12, 14, 17]. The $v_\perp^{\rm turb}$ measured by PCR is due to the turbulence velocity in the plasma frame superimposed on the $E_r \times B$ velocity. The E_r has been deduced from the $v_\perp^{\rm turb}$ by assuming that the $E_r \times B$ velocity dominates in the $v_\perp^{\rm turb}$ [11]. In a series of repeated ohmic discharges in this experiment, the profile of the radial electric field from $r/a \sim 0.54$ to $r/a \sim 0.79$, i.e. covering the $q = 2$ and $q = 3$ surfaces, has been measured by scanning the microwave frequency of the PCR pulse by pulse.

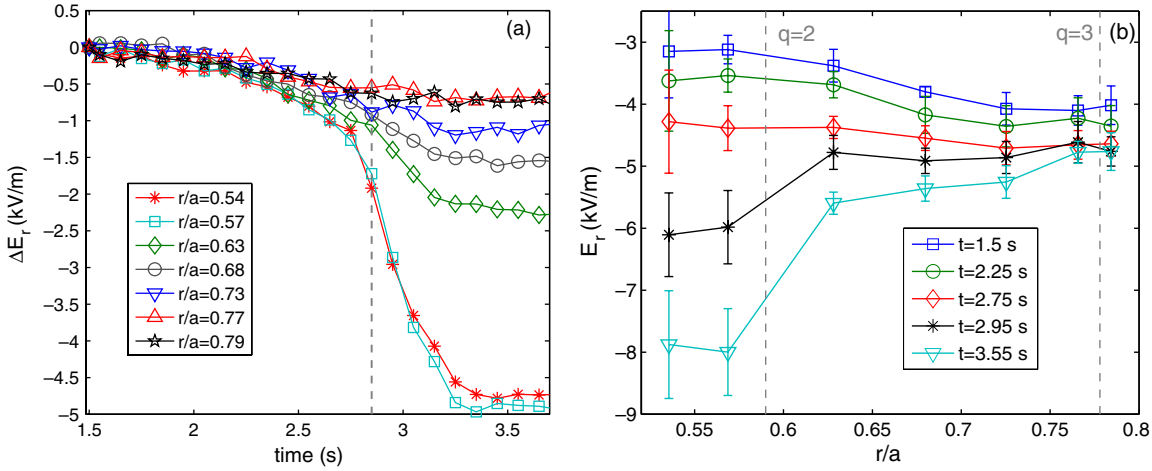

Figure 2. (*a*) The evolutions of the ΔE_r in the experiment where the ΔE_r is the quantity with the E_r during the application of the RMP field minus that before the field. The vertical dashed line indicates the time of the 2/1 mode excitation. (*b*) The profiles of the E_r at different time slices in this experiment. The vertical dashed lines indicate the positions of $q = 2$ and $q = 3$ surfaces.

2.2. Influence of the 5 kHz counter-rotating RMP field on the radial electric field

An overview of the experiment is shown in figure 1. The DED coil current ($I_{\rm DED}$), inducing the counter-rotating RMP field, is applied at 1.5 s, then ramps up to 0.56 kA in 2 s and stays at the flattop for 0.5 s as shown in figure 1(*c*), where only the amplitude of this oscillaing current is shown. When the $I_{\rm DED}$ ramps up to about 0.4 kA at the time of 2.85 s, an $m/n = 2/1$ tearing mode is excited and the core temperature, measured by the electron cyclotron emission (ECE) diagnostics [18], shows an abrupt decrease while the core line-averaged density does not change due to the density feedback control. Figure 1(*d*) shows the evolutions of the E_r at three different radial positions. Before the application of the rotating field, the radial electric fields are negative. This negative E_r points from the plasma edge to the core and induces an $E_r \times B$ velocity in the EDD direction. As the $I_{\rm DED}$ increases, the E_r slowly decreases. This means that the E_r becomes more negative with the application of the 5 kHz counter-rotating field.

Figure 2(*a*) shows the time evolutions of ΔE_r. Here, ΔE_r is the change in the radial electric field, defined by $\Delta E_r = E_r^{\rm RMP} - E_r^0$, where $E_r^{\rm RMP}$ (E_r^0) is the radial electric field with (before) the application of the rotating field. Figure 2(*b*) shows the profiles of the E_r at different time slices. The E_r profile shows two distinct evolution stages. In the first stage, i.e. from 1.5 to 2.75 s, the ΔE_r at all radial positions have a similar decrease and thus the profile of the E_r shifts downside as a whole as seen in figure 2(*b*). In the second stage, i.e. from 2.75 to 3.5 s, the ΔE_r at these positions have different decrease rates, which are faster for the positions closer to the $q = 2$ surface. In particular, the ΔE_r at the two outer positions, i.e. $r/a = 0.77$ and $r/a = 0.79$, nearly have no changes in this second stage. Thus the evolutions of the E_r profile are distinct from those in the first stage. It can be seen in figure 2(*b*) that the values of the E_r at the two outer positions in the second stage are the same as those at the time of 2.75 s while the value of the E_r at the inner position around $r/a = 0.55$ decreases from about -4.2 to -8 kV m^{-1} in the second stage.

By applying the 5 kHz counter-rotating RMP field in the ohmic plasmas, the change in the E_r is negative even before the 2/1 mode excitation as shown in figure 2(*a*). This result is different from the observations in previous experiments with the application of a static or low frequency (∼1 kHz) rotating RMP field on TEXTOR, where the changes in the E_r were always positive. The observation of the 2/1 mode excitation in the present experiment implies that this negative ΔE_r with the application of the 5 kHz counter-rotating field may be due to the resonant EM force [19–23] localized around the $q = 2$ surface. In order to improve our understanding, the experimental results have been compared with the simulation performed by the reduced MHD code 4FC.

3. Comparisons between the experiment and the 4FC simulations

The 4FC code, first introduced in [15], solves a reduced model of the four-field equations [24] by omitting the curvature term. In this work, equations (1)–(4) in [15] have been solved by the 4FC for the comparisons. The simulation is quasi-linear in the sense that the perturbation harmonic can, by interacting with themselves, modify the equilibrium profiles. More details of the 4FC code can be found in [15] and the limitations of this quasi-linear code are discussed in section 4.2. The input profiles in the 4FC for this work are shown in figure 3. The pressure ($p_{\rm e}$) profile is formed using the density profile measured by an HCN interferometer and a constant electron temperature ($T_{\rm e}$) of 0.8 keV since the $T_{\rm e}$ was assumed to be constant in deducing the four-field equations in [24]. The choice of the specific value of $T_{\rm e}$ is discussed in section 4.1. The η is the Spitzer resistivity with a neoclassical modification [25]. The q profile is assumed to take a form of $q = q(0)[1 + (r/a)^{\alpha}]^{\beta}$ and determined by considering $q(0)$, $q(a)$ and the position of $q = 2$, where $q(0)$ and $q(a)$ are the core and edge safety factors, respectively. Since the sawtooth is observed before the application of the rotating field, $q(0)$ is less than 1. In the present simulations, $q(0)$ is taken to be 0.65. Further discussion on the choice of $q(0)$ can be found in section 4.1. The $B_{\rm t}$ and $I_{\rm p}$ determine a cylindrical $q(a)$ of 4.7.

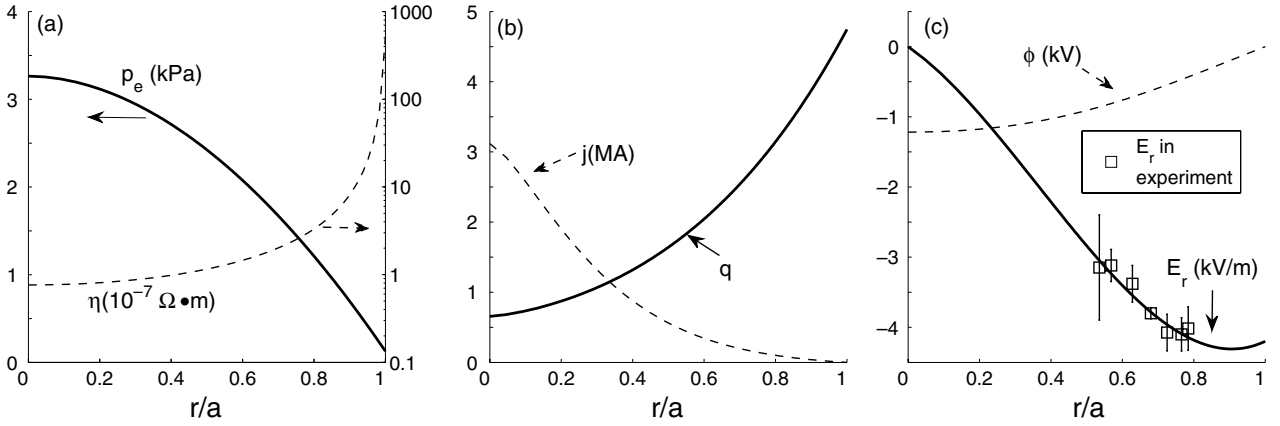

Figure 3. The input profiles in the 4FC code for the comparisons between experiment and simulation: (a) profiles of the electron pressure (p_e) and the resistivity (η), (b) profiles of the plasma current density (j) and the safety factor (q) and (c) profiles of the electric potential (ϕ) and the radial electric field (E_r).

The $q = 2$ surface is between $r/a = 0.53$ and $r/a = 0.62$ which is confirmed from the inversion of a 5 kHz oscillation in the ECE signal after the 2/1 mode excitation. Here, we set the surface of $q = 2$ at $r/a = 0.59$. The current (j) profile is derived from the q profile. With this current profile, both the 2/1 and 3/1 modes are stable before the application of the rotating field in the 4FC code. The electric potential (ϕ) profile is derived from the E_r profile, which is formed by fitting the experimental values of the E_r with a third order polynomial. The input parallel velocities are set to zero at all radial positions. The coefficients of the perpendicular, parallel viscosity and perpendicular heat transport are set to be the same value 8 $m^2\ s^{-1}$ everywhere. This value is similar to that estimated from the turbulence measurement (figure 15 in [11]).

The region for the numerical calculation is from $r/a = 0$ to $r/a = 1$. The boundary conditions in the present simulations are as follows:

(1) At $r/a = 0$, the first derivative of all quantities are set to zero.

(2) At $r/a = 1$, all the equilibrium quantities ($m/n = 0/0$) take the same values as the initial equilibrium ones.

(3) At $r/a = 1$, all the perturbations ($m/n \neq 0/0$) are zero except for the perturbed magnetic flux (ψ_{mn}). The condition for ψ_{mn} at $r/a = 1$ is

$$\frac{\partial \psi_{mn}}{\partial r}|_{r/a=1} + \frac{m}{r}\psi_{mn}|_{r/a=1} = \frac{2m}{r}\psi^{\rm vac}_{mn}(t)|_{r/a=1} = \frac{2m}{r}\psi_0 \frac{t}{t_{\rm coil}} e^{-iwt}|_{r/a=1} \quad (1)$$

which is a mixture of Dirichlet and Neumann conditions derived in [15]. Here, the term $t/t_{\rm coil}$ mimics the ramping up of the field amplitude in the experiment (figure 1(c)) where $t_{\rm coil}$ is a constant time, the term e^{-iwt} denotes a rotating field with an angular frequency of w and ψ_0 a constant magnetic flux.

Since the 2/1 mode excitation is observed in the experiment, the first simulation is by applying an $m/n = 2/1$ perturbation in the 4FC code.

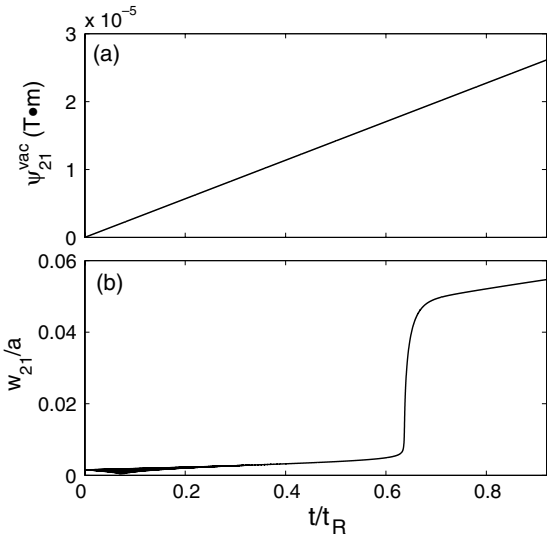

Figure 4. Overview of the simulation by applying a single 2/1 perturbation in the 4FC code: (a) the amplitude of the applied 5 kHz counter-rotating 2/1 perturbation and (b) the width of the 2/1 island. The 2/1 mode is excited at $t = 0.63t_{\rm R}$.

3.1. The comparison by applying a single 2/1 perturbation in the 4FC

An overview of the simulation by applying a single 2/1 perturbation with a frequency of 5 kHz in the 4FC is shown in figure 4. The amplitude of the $\psi^{\rm vac}_{21}(t)$ in equation (1), indicating the strength of the 2/1 perturbation, slowly ramps up to 2.6×10^{-5} T m in a time of $0.9t_{\rm R}$. Here, $t_{\rm R}$ is the resistive diffusion time defined by $t_{\rm R} = \mu_0 a^2/\eta_{q=2}$ where μ_0 is the vacuum permeability and $\eta_{q=2}$ the resistivity at the $q = 2$ surface. Figure 4(b) shows that the normalized width of the 2/1 magnetic island has a jump from less than 0.01 to 0.05 at about $t/t_{\rm R} = 0.63$, which is indicated as the time of the 2/1 mode excitation.

Figure 5(a) shows the evolutions of the ΔE_r at the radial positions where the E_r are measured in the experiment and figure 5(b) shows the profiles of the E_r at different time slices. With the application of the 2/1 perturbation, the E_r becomes more negative. This observation is consistent with

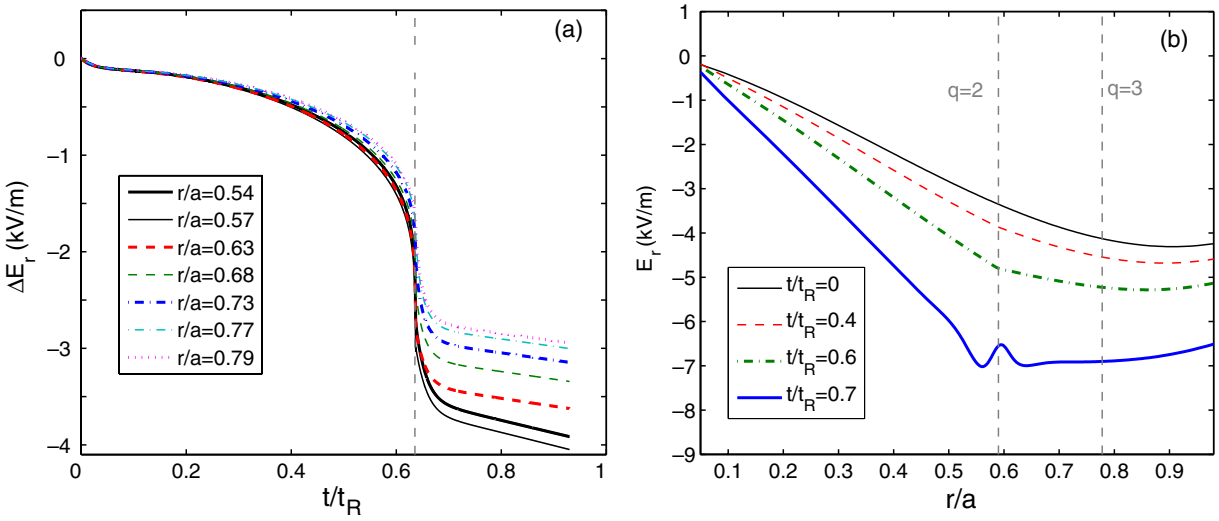

Figure 5. The results in the simulation by applying a single 2/1 perturbation in the 4FC code: (*a*) the evolutions of the ΔE_r at the radial positions where the E_r are measured in the experiment. The vertical dashed line indicates the time of the 2/1 mode excitation in this simulation. (*b*) The E_r profiles at different time slices. The two vertical dashed lines indicates the positions of the $q = 2$ and $q = 3$ surfaces, respectively.

the experimental result. However, the second evolution stage of the experimental E_r profile, where the E_r has a significant decrease around the $q = 2$ surface while there is no change of the E_r around the $q = 3$ surface (section 2.2), is not observed in this simulation.

3.2. The comparison by applying 2/1 and 3/1 perturbations in the 4FC

Considering the fact that there is a strong $m/n = 3/1$ perturbation in the field induced by the DED in the $m/n = 3/1$ configuration, we have performed another simulation by applying both 2/1 and 3/1 perturbations in the 4FC code. An overview of this simulation is shown in figure 6. The amplitudes of the 2/1 and 3/1 perturbations are set to be the same in this simulation. This is consistent with the fact that the strengths of the 2/1 and 3/1 components in the DED-field are comparable at the plasma edge when the DED is operated in the $m/n = 3/1$ configuration [8]. The 2/1 mode is excited at the time of $t/t_R = 0.83$ while the 3/1 mode excitation happens at the beginning of the application of the 3/1 perturbation. Figure 7 shows the evolutions of the MHD frequencies ($f_{m/n}$) [4]. Here, $f_{m/n}$ is defined by $f_{m/n} = [\frac{m}{2\pi r}(E_r + \frac{\nabla p_e}{ne})/B]|_{r=r_s}$, where r_s indicates the radius of the mode resonant surface. It can be seen from the figure that the 3/1 MHD mode frequency before the application of the perturbation is about −4.85 kHz, very close to the frequency of the counter-rotating field, i.e. −5 kHz. This explains why the 3/1 mode is very easy to excite in the simulation.

Figure 8(*a*) shows the evolutions of the ΔE_r and figure 8(*b*) shows the E_r profiles. The evolutions of the E_r profile, like the experimental observations, also have two distinct stages. In the first stage from $t/t_R = 0$ to $t/t_R = 0.3$, the ΔE_r at all positions show a similar decrease although this decrease mainly happens from $t/t_R = 0$ to $t/t_R = 0.1$ due to the 3/1 mode excitation. However, in the second stage after $t/t_R = 0.3$, the decrease rates of the ΔE_r are faster for the

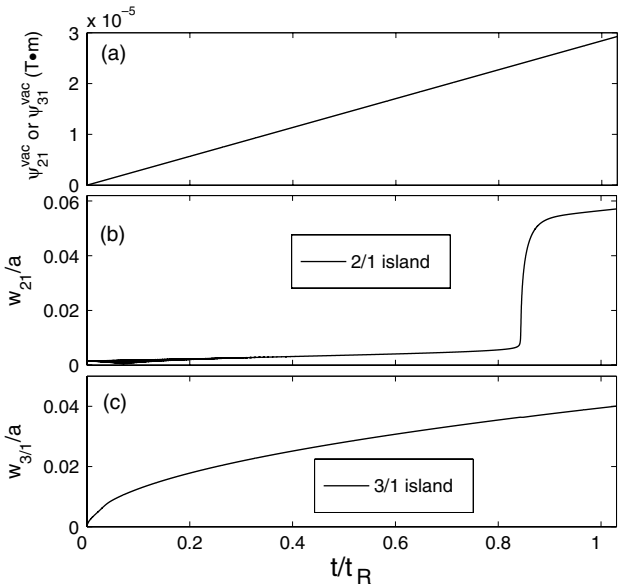

Figure 6. Overview of the simulation by applying 2/1 and 3/1 perturbations in the 4FC code: (*a*) the amplitudes of the 2/1 or 3/1 perturbations, (*b*) the width of the 2/1 island and (*c*) the width of the 3/1 island. The 2/1 mode is excited at $t = 0.83t_R$.

positions closer to the $q = 2$ surface. Further, the E_r at the two outer positions, i.e. $r/a = 0.77$ and $r/a = 0.79$, nearly have no changes in this second stage even after the 2/1 mode excitation. These results are qualitatively consistent with the experimental observations as discussed in section 2.2.

4. Discussion

4.1. Discussion on the results

The 4FC code has been used to help understand the mechanism responsible for the E_r change in our experiment. In the 4FC,

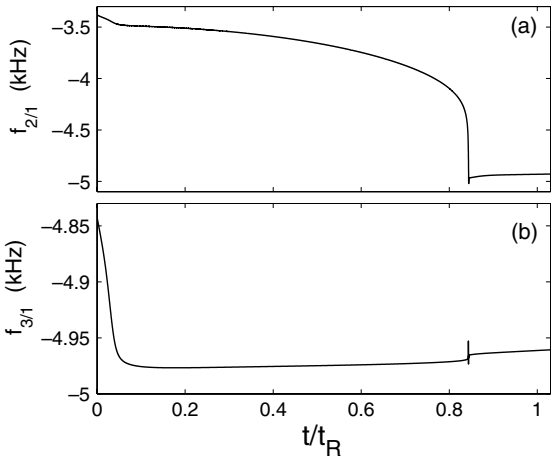

Figure 7. The evolutions of the MHD frequencies for 2/1 mode in (*a*) and 3/1 mode in (*b*).

the mechanism responsible for the E_r change can be seen from the equation of the vorticity (U) [15],

$$\frac{\partial \bar{U}}{\partial t} + \langle[\tilde{\phi}, \tilde{U}]\rangle + \langle[\tilde{j}, \tilde{\psi}]\rangle = \nu_\perp \nabla_\perp^2 (\bar{U} - \bar{U}_0) \qquad (2)$$

where the bar indicates an equilibrium ($m/n = 0/0$) quantity, the tilde indicates a perturbed ($m/n \neq 0/0$) quantity and $\langle \cdots \rangle$ represents the flux surface average. The term in the right-hand side is related to the viscous force. The third term in the left-hand side, expressed using Poisson's bracket, is related to the $\tilde{J} \times \tilde{B}$ EM force [19–23] in which mainly the force in the poloidal direction is responsible for the E_r change in the four-field model [24]. The second term in the left-hand side, related to the Reynolds stress, has no contribution to the E_r change in the present simulations. It should be noted that the Reynolds stress may be important in the process of the RMP field penetration as shown in [26]. This EM force, localized around the resonant surface due to the direct coupling between the RMP fields and plasma [19], always tries to make the resonant mode rest in the frame of the external RMP field. Since both of the MHD frequencies for the 2/1 and 3/1 modes are larger than −5 kHz, the frequency of the external field (figure 7), the resonant EM forces around the $q = 2$ or $q = 3$ surface with the application of the rotating field will reduce the E_r as observed in the experiment (figure 2) and in the simulations (figures 5 and 8).

The first evolution stage of the E_r profile in the experiment has been observed in both simulations in section 3. However, the second evolution stage of the experimental E_r profile can only be observed in the second simulation where both the 2/1 and 3/1 perturbation are applied in the 4FC (figure 8). Figure 9 shows the radial profiles of the EM force density ($F_{j\times B}$) at different time slices in this second simulation. In this figure, a positive force leads to a negative E_r. At an early time, e.g. $t/t_R = 0.05$, a positive force localizes on the $q = 3$ surface although no force is observed on the $q = 2$ surface. This positive force on the $q = 3$ surface is responsible for the change in the E_r profiles in the first stage of the simulation as discussed in section 3.2. After the 3/1 mode excitation, the force on the $q = 3$ surface becomes negative as seen from the profile of $F_{j\times B}$ at $t/t_R = 0.2$ in figure 9 and a positive force on the $q = 2$ surface appears. As the amplitudes of the perturbations increase, this positive force on the $q = 2$ surface, responsible for the E_r change in the second stage of the simulation discussed in 3.2, increases while the strength of the negative force on the $q = 3$ surface also increases. This increasing negative EM force balances the increasing viscous force around the $q = 3$ surface so that the E_r around the $q = 3$ surface cannot be changed in the second stage.

Based on the results of the simulations, a possible explanation of the E_r evolutions in the experiment can be given. With the application of the 5 kHz counter-rotating RMP field, the changes in the E_r from the $q = 2$ to $q = 3$ surface are similar, mainly due to a positive resonant EM force on the $q = 3$ surface. After the 3/1 mode excitation, the E_r around the $q = 3$ surface cannot be changed due to the balance between a negative EM force and the viscous force around this surface while the E_r inside the $q = 3$ surface can be further reduced due to the localized EM force on the $q = 2$ surface. In this explanation, edge stochastization is not necessary. The theory in [27] predicts that a counter-rotating RMP field could induce negative electric field even in the stochastic region. Since there is no evidence of stochastization or no stochastization based on the present experimental result, the contribution of the stochastization to the change in the E_r observed in the first stage cannot be excluded. Nevertheless, the evolution of E_r in the second stage clearly indicates the localized resonant force around the $q = 2$ surface as observed in the simulations.

In the above explanation of the E_r evolution, the excitation of the 3/1 mode is needed to explain why the E_r around the $q = 3$ surface has no change after 2.75 s in the experiment as shown in figure 2. In the experiment, no drop in the T_e and no flatting of the T_e profile around the $q = 3$ surface are observed before the excitation of the 2/1 mode at 2.85 s (figure 1(*b*)). According to the theory in [28], there is a critical island width below which the island gives rise to no local flatting of the electron temperature profile. This critical island width (W_c), given in [28], is estimated to be

$$\frac{W_c}{a} \sim \left(\frac{\kappa_\perp}{\kappa_\parallel}\right)^{1/4} \left(\frac{1}{\epsilon\, sn}\right)^{1/2} \qquad (3)$$

where $\kappa_\perp$ is the perpendicular heat diffusivity, $\kappa_\parallel$ is the parallel heat diffusivity, ϵ is the inverse aspect ratio, $s = rq'/q$ is the magnetic shear and n is the toroidal mode number. A simple estimation of the critical width for the 3/1 island gives $W_c/a \sim 0.041$ by taking $\kappa_\perp = 8\,\mathrm{m^2\,s^{-1}}$ and $\kappa_\parallel \sim v_{T_e}\lambda_\parallel \sim v_{T_e} q R_0 = 3.1 \times 10^7\,\mathrm{m^2\,s^{-1}}$ with $T_e = 0.2$ keV at the $q = 3$ surface measured by the ECE diagnostics in the experiment. Here, $v_{T_e} = \sqrt{T_e/m_e}$ is the electron thermal velocity and $\lambda_\parallel$ the parallel connection length. Figure 6(*c*) shows that the normalized 3/1 island width in the second simulation is smaller than 0.4, which is lower than the critical width estimated using equation (3). This may explain why no drop in the T_e and no flatting of the T_e profile around the $q = 3$ surface are observed in the experiment. On the other hand, the critical width for the 2/1 island is estimated to be $W_c/a \sim 0.047$ using $\kappa_\parallel \sim 2.9 \times 10^7\,\mathrm{m^2\,s^{-1}}$ (with $T_e = 0.4$ keV on the $q = 2$ surface) in equation (3). Figure 6(*b*) shows that the normalized 2/1 island width after mode excitation, e.g. at $t/t_R = 0.9$, is about 0.055, which is larger than the critical island width.

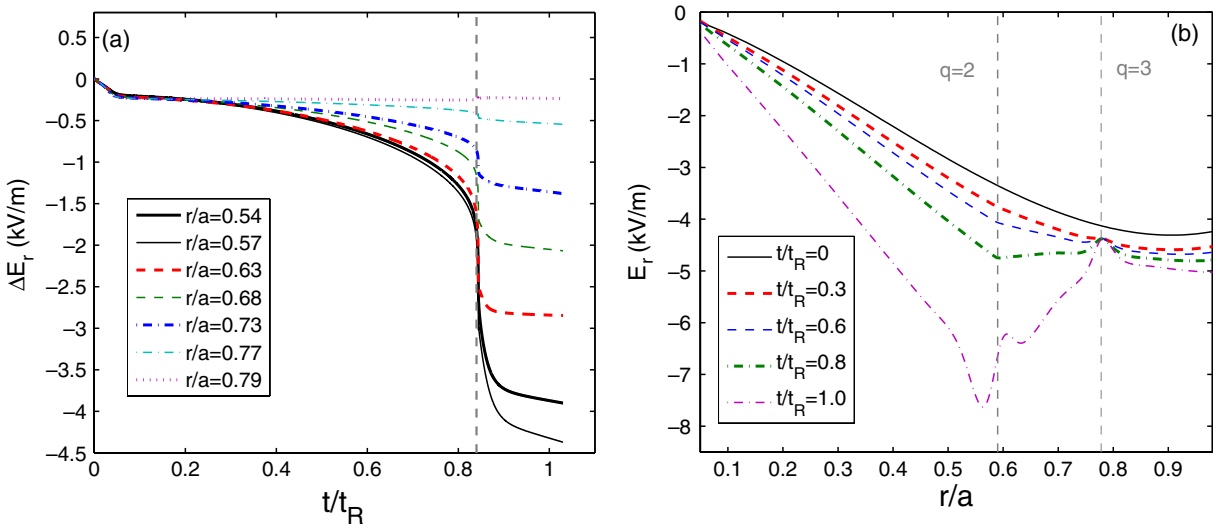

Figure 8. The results in the simulation by applying 2/1 and 3/1 perturbations in the 4FC code (*a*) the evolutions of the ΔE_r. The vertical dashed line indicates the time of the 2/1 mode excitation in this simulation. (*b*) the E_r profiles at different time slices. The two vertical dashed lines indicate the positions of the $q = 2$ and $q = 3$ surfaces, respectively.

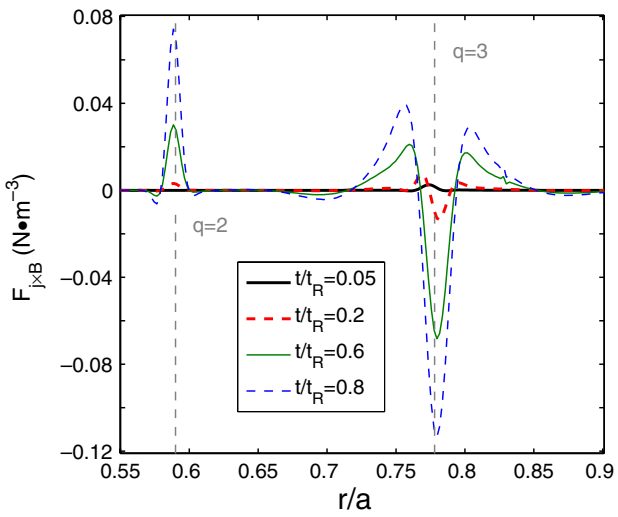

Figure 9. The radial profiles of the EM force density ($F_{j\times B}$) at different time slices in the simulation by applying 2/1 and 3/1 perturbations in the 4FC code. The two vertical dashed lines indicate the positions of the $q = 2$ and $q = 3$ surfaces, respectively.

According to the theory in [28], this size 2/1 island can induce the flatting or decrease in T_e around the $q = 2$ surface as observed in the experiment.

Lastly, the choice of the specific value of the input temperature and $q(0)$ in the simulations should be discussed. The four-field model in [24] was deduced based on the assumption of a constant temperature. The equation of the pressure in the model in fact came from the density evolution equation. By considering this, a constant temperature of 0.8 keV has been used in the present simulations. We have performed another simulation using $T_e = 0.4$ keV, the temperature at the $q = 2$ surface and $T_e = 0.5$ keV, the volume-averaged temperature. The results show that the different input temperatures do not change the main findings: the second evolution stage of the E_r profile observed in the experiment can only be seen in the simulation by applying both 2/1 and 3/1 perturbations in the 4FC code. In the present work, we have assumed that the q profile takes the form $q = q(0)[1 + (r/a)^{\alpha}]^{\beta}$. On TEXTOR, the core safety factor is generally larger than 0.5 [29]. It is found that only the profiles with $q(0) < 0.75$ are free of the 2/1 and 3/1 unstable modes before the application of the RMP field. Considering the fact that the tearing mode linear stability parameter is sensitive to the q profile, other simulations using the q profiles with $q(0) = 0.5$ and $q(0) = 0.7$ have been performed. The results show that the above mentioned main findings are not changed using different values of $q(0)$ in the 4FC code.

4.2. Limitations of the present 4FC modelling

The neoclassical effects are believed to be responsible for the radial electric field profile as shown in [30–36]. The present simulations performed by the 4FC code are without neoclassical effects so they might not contain all the physics. As previously stated, the E_r change in the 4FC code is mainly related to the poloidal force. In this work, the neoclassical poloidal flow damping effect [37] is not included, thus it is expected that the simulations will give smaller penetration thresholds than those in the experiment according to the theory in [20]. Figure 6(*b*) shows that the penetration threshold for 2/1 mode in the second simulation is about 1 G calculated using the formula $b_r = \frac{m}{r}\psi$, where b_r is the perturbed radial magnetic field. This threshold value is about one order smaller than that, approximately 10 G [38], in the experiment.

Since a cylindrical geometry is assumed in the 4FC modelling, it is certain that the physics of the toroidal mode coupling cannot be captured by the present simulations. In cylindrical geometry, an $m/n = 2/1$ RMP field can only exert a torque at the $q = 2$ rational surface. In toroidal plasmas, however, an $m/n = 2/1$ field can exert a torque on the $q = 3$ surface due to the coupling of different poloidal harmonics. This kind of geometry effect could be important for the RMP physics, as noted in analytical theory [39] and numerical calculation [40].

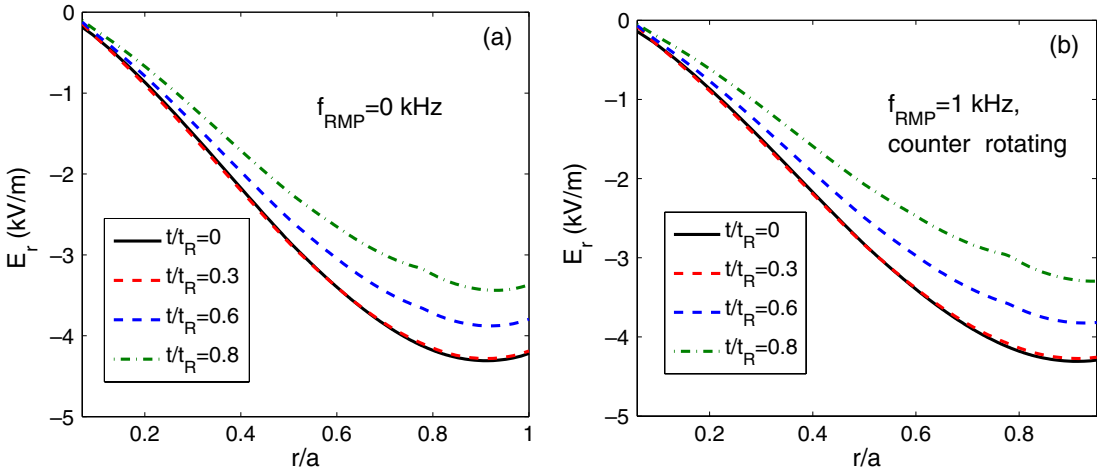

Figure 10. The E_r profiles in 4FC simulations by applying 2/1 and 3/1 perturbations. (*a*) With a static field, (*b*) with a 1 kHz counter-rotating field. The other parameters in the simulations are similar to those in figure 8.

As shown in Rutherford's paper [41] and more recently in [42, 43], the nonlinear island evolution requires multiple harmonics for the perturbed current density while the magnetic flux can be approximated with only one harmonic. This implies that the correct nonlinear evolution of the magnetic island can be properly simulated only when a sufficient number of poloidal harmonics are taken into account. This has been tested and validated by some simulations, see, for example, [44]. Due to the quasi-linear nature, the present 4FC model cannot properly treat the nonlinear evolution of island saturation. On the other hand, we believe the nonlinear island saturation physics are not playing key roles in the rotating RMP experiment. The key physics in the experiment are that (i) the frequency of the excited tearing mode matches the RMP frequency; and (ii) the $E \times B$ rotation and hence the radial electric field are determined by the torque balance between the EM force and the viscous force [20]. The analysis has shown that the frequency spectrum of the magnetic flux in our simulations actually displays a mode with a frequency of 5 kHz. This indicates the first key physics outlined above can be captured by the present modelling. The discussion in section 4.1 shows that the 4FC can also well capture the second key physics to a good degree. These explain why the present modelling can qualitatively reproduce the experimental results. Furthermore, other simulations have been performed by applying 0 kHz, counter-rotating 1 kHz and co-rotating 1 kHz RMP fields in the 4FC code, respectively. The results show that the changes in E_r are positive with the applications of the three fields. Figure 10 shows the E_r profiles when a static field or 1 kHz counter-rotating field is applied in the 4FC code. The positive changes in E_r observed in these simulations are consistent with the previous experimental observations with the applications of static, counter-rotating or co-rotating fields on TEXTOR [5, 9].

5. Conclusion

In conclusion, the radial electric field in ohmic plasma has been changed with the application of a 5 kHz counter-rotating RMP field, induced by the DED in the $m/n = 3/1$ configuration on TEXTOR. Two distinct evolution stages of the E_r profile have been determined in the experiment. In the first stage, the E_r profile from the $q = 2$ to $q = 3$ surface shifts downside as a whole as the amplitude of the DED-field increases. In the second stage, the E_r around the $q = 2$ surface have significant decreases while the E_r around the $q = 3$ surface have no changes even after the excitation of an $m/n = 2/1$ tearing mode. The 4FC, a reduced MHD code, has been used for the comparison between experiment and simulation. Two simulations have been performed. In the first simulation, a single 2/1 perturbation is applied in the 4FC. The result shows that the second evolution stage of the E_r profile cannot be observed in this simulation. However, when the 2/1 and 3/1 perturbations are applied in the 4FC in the second simulation, the two distinct evolution stages are observed. A possible explanation on the evolutions of the E_r profile in the experiment has been given: the evolution of the E_r profile in the first stage is due to a positive EM force at the $q = 3$ surface or even from a contribution of edge stochastization while the E_r profile evolution in the second stage is attributed to a positive EM force on the $q = 2$ surface along with a negative EM force on the $q = 3$ force.

Acknowledgments

This work is funded by the Helmholtz Association within the framework of the Helmholtz-University Young Investigators Group VH-NG-410.

References

[1] Evans T. *et al* 2006 *Nature Phys.* **2** 419
[2] Liang Y. *et al* 2007 *Phys. Rev. Lett.* **98** 265004
[3] Liang Y. *et al* 2010 *Nucl. Fusion* **50** 025013
[4] Koslowski H.R. *et al* 2006 *Nucl. Fusion* **46** L1
[5] De Bock M.F.M. *et al* 2008 *Nucl. Fusion* **48** 015007
[6] Terry P.W. 2000 *Rev. Mod. Phys.* **72** 109
[7] Finken K.H. *et al* 1997 *Fusion Eng. Des* **37** 335
[8] Finken K.H. *et al* 2005 The structure of magnetic field in the TEXTOR-DED *TEXTOR Report IPP*

[9] Finken K.H. *et al* 2005 *Phys. Rev. Lett.* **94** 015003
[10] Xu Y. *et al* 2007 *Nucl. Fusion* **47** 1696
[11] Krämer-Flecken A. *et al* 2006 *Nucl. Fusion* **46** S730
[12] Krämer-Flecken A. *et al* 2004 *Nucl. Fusion* **44** 1143
[13] Krämer-Flecken A. *et al* 2010 *Rev. Sci. Instrum.* **81** 113502
[14] Soldatov S., Krämer-Flecken A. and Zorenko O. 2011 *Rev. Sci. Instrum.* **82** 033513
[15] Nardon E. *et al* 2010 *Nucl. Fusion* **50** 034002
[16] Horton W. 1999 *Rev. Mod. Phys.* **71** 735
[17] Vershkov V.L. *et al* 1999 *Rev. Sci. Instrum.* **70** 1700
[18] De Vries P.C. *et al* 1997 *Plasma Phys. Control. Fusion* **39** 439
[19] Fitzpatrick R. 1993 *Nucl. Fusion* **33** 1049
[20] Fitzpatrick R. 1998 *Phys. Plasmas* **5** 3325
[21] Waelbroeck F.L. 2003 *Phys. Plasmas* **10** 4040
[22] Boozer A.H. 2009 *Phys. Plasmas* **16** 052505
[23] Yu Q. *et al* 2008 *Nucl. Fusion* **48** 024007
[24] Hazeltine R.D. *et al* 1985 *Phys. Fluids* **28** 2466
[25] Wesson J. 2004 *Tokamaks* 3rd edn (Oxford: Oxford University Press)
[26] Militello F. and Waelbroeck F.L. 2009 *Nucl. Fusion* **49** 065018
[27] Kaveeva E. and Rozhansky V. 2012 *Nucl Fusion* **52** 054011
[28] Fitzpatrick R. 1995 *Phys. Plasmas* **2** 825
[29] Koslowski H.R. *et al* 1997 *Plasma Phys. Control. Fusion* **39** B325
[30] Kaveeva E., Rozhansky V. and Tendler 2008 *Nucl. Fusion* **48** 075003
[31] Tokar M.Z. *et al* 2008 *Phys. Plasmas* **15** 072515
[32] Unterberg B. *et al* 2007 *J. Nucl. Mater.* **363–365** 698
[33] Rozhansky V. *et al* 2010 *Nucl. Fusion* **50** 034005
[34] Rozhansky V. *et al* 2011 *Nucl. Fusion* **51** 083009
[35] Park G. *et al* 2010 *Phys. Plasmas* **17** 102503
[36] Becoulet M. *et al* 2012 *Nucl. Fusion* **52** 054003
[37] Stix T.H. 1973 *Phys. Fluids* **16** 1260
[38] Wolf R.C. *et al* 2005 *Nucl. Fusion* **45** 1700
[39] Fitzpatrick R. 2009 *Phys. Plasmas* **16** 032502
[40] Park J.K., Schaffer M.J., Menard J.E. and Boozer A.H. 2007 *Phys. Rev. Lett.* **99** 195003
[41] Rutherford P.H. 1973 *Phys. Fluids* **16** 1903
[42] Escande D.F. and Ottaviani M. 2004 *Phys. Lett.* A **323** 278
[43] Militello F. and Porcelli F. 2004 *Phys. Plasmas* **11** L13
[44] Loureiro N.F. *et al* 2005 *Phys. Rev. Lett.* **95** 235003